Linear Collider Collaboration Tech Notes

Study of Alternative Optics for the NLC Prelinac Collimation section

March 2001

Yuri Nosochkov, Pantaleo Raimondi, Tor Raubenheimer

Stanford Linear Accelerator Center
Stanford, California

Abstract: In this note, we describe a study of alternative optics for the NLC pre-linac collimation and bunch compressor sections. The advantage of the new design is a significant reduction of effective emittance growth and a less complex collimation system compared to the ZDR type design. In the new collimation section design, only energy collimation is performed, and the betatron collimation will take place upstream the collimation section, just after the damping rings. The new optics described in this note are not exactly the most recent NLC optics, but were, in part, the basis for the present optics.
.

Study of Alternative Optics for the NLC Pre-Linac Collimation Section *

Yuri Nosochkov, Pantaleo Raimondi and Tor Raubenheimer
Stanford Linear Accelerator Center, Stanford University, Stanford, CA 94309

Abstract

In this note, we describe a study of an alternative optics for the NLC pre-linac collimation and bunch compressor sections. The advantage of the new design is a significant reduction of effective emittance growth and a less complex collimation system compared to the ZDR type design [1]. In the new collimation section design, only energy collimation is performed, and the betatron collimation will take place upstream the collimation section, just after the damping rings. The new optics described in this note is not exactly the most recent NLC optics [2], but it was, in part, the basis for the present optics.

1 Pre-Linac Collimation Section

1.1 ZDR Type Design

Optics

The pre-collimation section based on the ZDR design [1], its lattice functions and phase advance are shown in Fig. 1 and 2. The collimation system in this design consists of interleaved horizontal and vertical spoilers and absorbers located in the four identical $-I$ cells in the beginning of the section. The first and second pairs of $-I$ cells are separated by phase advance of $\mu_x = \frac{5\pi}{2}, \mu_y = \frac{\pi}{2}$ to provide collimation at the phase of Interaction Point (IP) and Final Doublet (FD). Downstream of the $-I$ cells, the optics contains five 45° diagnostic cells for emittance measurement.

The ZDR $-I$ cells have large β-functions and non-zero dispersion and generate betatron and dispersive chromatic aberrations. The $(\frac{5\pi}{2}, \frac{\pi}{2})$ phase advance between the $-I$ pairs helps cancel the first order chromatic β-distortion, but local β-perturbations are rather large. To minimize these aberrations, seven families of sextupoles are placed symmetrically in the $-I$ cells to correct the betatron and dispersive chromaticity. Chromatic W-functions and second order dispersion after correction are shown in Fig. 3 and 4, respectively. The sextupoles also generate third order geometric aberrations which along with the residual chromatic effects may result in emittance growth.

Tracking

To evaluate emittance growth in the pre-linac collimation section, we tracked 10,000 particles using NLC version of DIMAD code [3]. The initial lattice functions were matched to the upstream optics, and the following set of 'nominal' beam parameters was used:

$$E = 8GeV, \quad \gamma\epsilon_{0x} = 3 \cdot 10^{-6}m, \quad \gamma\epsilon_{0y} = 3 \cdot 10^{-8}m, \quad \sigma_\delta = 0.26\%, \quad \sigma_z = 0.5mm, \qquad (1)$$

*Work supported by Department of Energy contract DE–AC03–76SF00515.

where E is the beam energy, $\gamma = E/mc^2$, ϵ_0 the initial emittance, σ_δ the rms relative energy spread σ_E/E, and σ_z the rms bunch length.

To evaluate a full optical bandwidth, we removed the aperture limitation in tracking to allow all particles reach the end of the beamline, and turned off the synchrotron radiation energy loss. The beam was tracked at various values of initial average momentum error $\delta = \frac{\Delta p}{p}$, and the final emittance was obtained using 'particle distribution analysis' in DIMAD. In case of large beam tails, their contribution may result in an overestimated emittance value. In this case we calculated the beam core emittance using the formula:

$$\epsilon = \frac{\sigma_{lum}^2}{\beta}, \tag{2}$$

where σ_{lum} is so called 'luminosity equivalent' rms beam size in DIMAD which under-emphasizes the effect of large tails, and β is the matched β-function.

Filamentation

The non-linear chromatic and geometric aberrations may distort the initial 'matched' ellipse-like beam phase space and displace particles from their phase trajectories. This distortion will not instantly change the beam phase space area, i.e. the emittance, but the distorted phase space will become a part of a new larger matched ellipse and the particles will start moving along the new phase trajectories. Due to energy dependence of phase advance, particles with different energies will eventually spread along the new phase trajectories and fill the entire new matched ellipse. This results in filamentation and emittance growth. It is important to verify this effect in order to accurately predict the final emittance at IP.

One way to estimate emittance growth with filamentation is to allow the beam travel enough distance for filamentation to take place. To use this method for the ZDR pre-linac collimation section, we extended the last five 45° diagnostic FODO cells by 1000 more cells. An analytic estimate and a simple test described below showed that this number of cells is enough for the filamentation to take place. The extra cells compose a pure quadrupole highly periodic non-dispersive matched optics which contribution to emittance growth is negligible.

In analytic estimate, we used the following first order formula for energy dependent phase advance in a FODO cell:

$$\Delta\mu = \mu(\delta) - \mu(0) = -2\delta \tan\frac{\mu}{2}, \tag{3}$$

where μ is phase advance across one cell. We assumed that particles will spread across the full phase ellipse after N-cells where $N\,|\Delta\mu| = \pi$ for $\delta = \pm\sigma_\delta$. This results in

$$N = \frac{\pi}{2\sigma_\delta \tan\frac{\mu}{2}}. \tag{4}$$

According to this estimate, one would need $N \approx 1460$ cells for $\sigma_\delta = 0.26\%$ and $\mu = 45°$.

To verify this estimate, we used DIMAD to calculate emittance as a function of N extension cells. In this test we used the nominal beam (Eq. 1) with an average $\delta = -4\%$. The results are shown in Fig. 5 and indicate that emittance grows almost linearly with N before it saturates. The Fig. 5 shows that at about $N = 1000$ cells filamentation is complete.

All emittance calculations presented in this paper include filamentation using the above method of tracking in an extended optics.

Emittance

Fig. 6 shows emittance growth as a function of δ for the ZDR type pre-linac collimation optics with bends and sextupoles turned off. It indicates that large β-functions in the quadrupoles ($\beta_y = 750m,\ \beta_x = 200m$) generate significant chromaticity and huge emittance growth. The results for complete optics including bends and chromaticity correcting sextupoles are shown in Fig. 7. The vertical chromatic emittance growth is too large and needs to be reduced. Besides chromaticity, the sextupoles also generate third order geometric aberrations which contribute to the emittance growth. This effect is significantly amplified at larger emittance as shown in Fig. 8, where the initial emittance is increased 10 times. Fig. 9 shows emittance growth vs. beam energy spread.

Based on the above calculations, we conclude that despite the sextupole correction, chromatic aberrations from quadrupoles with large vertical β-functions are still significant. To reduce emittance growth, we will attempt to modify the ZDR type collimation optics in such a way that:

- peak β-functions are significantly reduced
- sextupole geometric aberrations are canceled
- chromatic betatron and dispersive effects are minimal.

1.2 Alternative Design

Optics

The suggested alternative design considerably simplifies the pre-linac collimation optics, but it only includes the energy collimation system, and the betatron collimation is planned to take place upstream just after the damping rings. The new optics, lattice functions and phase advance are shown in Fig. 10 and 11. This optics contains four 45° diagnostics cells which are matched to two identical $-I$ cells where the collimators will be placed. The number of diagnostic cells can be increased if necessary. The optics is matched to the adjacent upstream and downstream NLC sections. All optical matching including chromatic correction has been done using MAD code [4].

Compared to the ZDR type design, the maximum vertical β-function in the new $-I$ cells is significantly reduced, from 750 to $100m$. For energy collimation, two horizontal bends are placed on either side of the second $-I$ cell to generate a closed dispersion bump with $\eta = -11.2cm$ in the middle of the cell. These two bends are the same magnets as in the downstream bunch compression section. The new bends are 34 times stronger than in the ZDR type design and generate an order of magnitude larger dispersion. Magnet parameters at 8 GeV for the new optics are listed in Table 1.

One $-I$ cell is sufficient for the collimation system, but two cells provide better conditions for a sextupole correction. Because of $-I$ transformation, sextupole geometric aberrations are automatically canceled for each pair of identical sextupoles placed at identical positions in the two $-I$ cells. Three such sextupole pairs are used in the new optics, with one pair placed at two $\beta_y = 100m$ peaks and two pairs at four $\beta_x \approx 15m$ peaks. Note that sextupoles in the first $-I$ cell with zero dispersion do not correct chromaticity, but cancel geometric aberrations generated in the second cell sextupoles. The strengths of the sextupoles have been optimized to minimize chromatic betatron distortions (W-functions) and second order dispersion. These functions after correction are shown in Fig. 12 and 13. Compared to the ZDR type design, the new sextupoles are about 5 times weaker because of larger dispersion and less quadrupole chromaticity. Sextupole parameters at 8 GeV are listed in Table 1.

Table 1: Magnet parameters at 8 GeV for the alternative pre-linac collimation section.

Magnet	Number	Length (m)	Pole-tip field (kG)	Aperture (cm)
Quadrupole				
QEF	3	0.26	2.6976	1.0
QED	4	0.26	2.6976	1.0
QCX1	4	0.26	1.8360	1.0
QCX2	8	0.26	1.8272	1.0
QCX3	4	0.26	1.7989	1.0
QMC1	1	0.26	4.8625	1.0
QMC2	1	0.26	2.6607	1.0
QMC3	1	0.26	3.9460	1.0
QMC4	1	0.26	4.0815	1.0
Dipole				
BA	2	1.0	9.3149	1.2
Sextupole				
SCX1	1	0.21	0.2745	1.0
SCX2	1	0.21	0.2745	1.0
SCX3	1	0.21	0.2745	1.0
SCX4	1	0.21	0.2745	1.0
SCY1	1	0.21	0.3565	1.0
SCY2	1	0.21	0.3565	1.0

Emittance

For emittance calculations with filamentation, we tracked particles through an extended section of one thousand 45° diagnostic cells attached after the $-I$ cells. First, we verified chromatic aberrations of the new optics without sextupole correction. Fig. 14 shows chromatic bandwidth with bends and sextupoles turned off. Evidently, the emittance growth due to horizontal betatron chromaticity from quadrupoles is negligible because of rather small horizontal β-function, but the vertical effect requires correction. The most contribution to the vertical chromaticity comes from a pair of quadrupoles with $\beta_y = 100m$. For an efficient correction, one pair of sextupoles is placed next to these quadrupoles. The other two sextupole pairs compensate the horizontal betatron and second order dispersive chromaticity.

Fig. 15 shows the bandwidth with the bends turned on and sextupoles off. Compared to Fig. 14, the vertical emittance has not changed by the bends, but the horizontal emittance has grown significantly. Clearly, this growth comes from the second and higher order dispersion, since there are no other significant aberrations from the bends. Note that these bends are much stronger than in the ZDR type optics.

With the sextupoles turned on, the second order dispersion is practically canceled at the end of the collimation section, as shown in Fig. 13. The resultant bandwidth is shown in Fig. 16 and 17 for the nominal and 10 times larger initial emittance. Compared to Fig. 7, the vertical emittance growth in the new design is significantly reduced, and the bandwidth is about $\pm 2\%$. Reduction of emittance growth at 10 times larger initial emittance indicates that geometric aberrations are

negligible and the relative chromatic contribution to emittance is reduced.

Emittance growth as a function of *rms* energy spread is shown in Fig. 18. Compared to Fig. 9, the vertical emittance growth is significantly smaller and the horizontal growth is of the same magnitude.

We conclude that the lower β_y-functions and the sextupole correction significantly increase the vertical chromatic bandwidth in the new optics. Second order dispersion caused by the stronger bends has been compensated using sextupoles, and the horizontal emittance is about flat within $\delta = \pm 2\%$.

One Bend Option

The primary purpose of the second bend in the new collimation section is to close the dispersion bump generated by the first bend. This way, the dispersion is automatically matched to the downstream bunch compressor optics which at present assumes zero initial dispersion. For the collimation system the second bend is not required because it is at the end of the section. However, without this bend, the linear and high order dispersion would not be zero in the beginning of the downstream bunch compressor and its optics would have to be modified to match this dispersion. More detailed analysis showed that the linear dispersion in the one bend optics can be matched to the bunch compressor optics. In fact, the first dispersion suppressor bend in the bunch compressor can be removed as well. In this case, the only bend in the collimation section would act as a remote dispersion suppressor bend for the bunch compressor. In total, two bends can be saved in this option.

The optics for this option was generated and analyzed. It required a modification of the quadrupole matching section between the collimation and bunch compressor sections. Same as above sextupole scheme was used to correct W-functions and second order dispersion in the collimation section. As a result of the absent second bend, the sextupoles get stronger by a factor of two to cancel the second order dispersion. Tracking in the combined collimation and bunch compressor sections showed a somewhat larger chromatic emittance growth compared to the 'two bend' collimation optics, possibly due to stronger sextupoles. Because of this result, we did not pursue this option further.

2 Pre-Linac Bunch Compressor Section

2.1 ZDR Type Optics

We also analyzed emittance growth in the pre-linac bunch compressor which is located after the collimation section. The ZDR type optics, lattice functions and phase advance in the bunch compressor are shown in Fig. 19 and 20. On the left side in Fig. 19, this section is matched to the new collimation section. The matching optics has been modified and the new quadrupole parameters are listed in Table 2. After the matching section, the bunch compressor consists of 44 arc cells and two dispersion suppressor bends to form a 180° arc. Two chicanes, compressor cells with RF-structures, and 45° diagnostic cells are located downstream of the 180° arc.

In the ZDR design, there are no sextupoles in the bunch compressor section. The chromatic betatron W-functions generated by the compressor quadrupoles are rather modest, as shown in Fig. 21. The two chicanes in the second half of the bunch compressor generate closed dispersion bumps including higher order dispersion, except possibly a small distortion due to the fringe fields. The 44 arc cells with two dispersion suppressor bends generate a closed linear dispersion bump as

Table 2: Quadrupole parameters at 8 GeV for the modified matching section in the pre-linac bunch compressor section.

Magnet	Number	Length (m)	Pole-tip field (kG)	Aperture (cm)
Quadrupole				
QMA1	1	0.26	4.1507	1.0
QMA2	1	0.26	1.8859	1.0
QMA3	1	0.26	7.0766	1.0
QMA4	1	0.26	7.0664	1.0

well, as shown in Fig. 19, but the arc is not achromatic in higher orders. Fig. 22 shows a modulation of the second order dispersion in the bunch compressor. This effect is caused by two dispersion suppressor bends located at either side of the arc which are not matched in non-linear orders to the periodic arc cells. This residual dispersion may cause horizontal emittance growth.

For emittance calculations, we used DIMAD to track 10,000 particles in the bunch compressor with the extension section for filamentation. The initial beam was matched to the upstream collimation optics, and the beam parameters listed in Eq. 1 were used. The extension section consisted of one thousand 45° diagnostic cells with zero dispersion. The resultant chromatic bandwidth is shown in Fig. 23. One can see that the horizontal chromatic emittance growth in the ZDR type optics is very large, mostly due to non-linear dispersion as will be shown below.

2.2 Sextupole Correction

The residual second order dispersion can be eliminated by using sextupoles in the compressor arc. Since the 44 periodic arc cells are naturally matched to each other, the mismatch of the second order dispersion comes from two dispersion suppressor bends at either side of the arc. A system of four sextupoles (two on each side of the arc) can be used to cancel this mismatch. The effect of these sextupoles is to match the second order dispersion to its natural periodic solution in the cells. Due to symmetry of the compressor arc, a symmetric sextupole scheme can be used with the identical sextupole pairs placed symmetrically at either side of the arc. The four sextupole scheme is sufficient for correction of the second order dispersion, but the sextupole geometric aberrations and chromatic betatron distortions may not cancel. It is therefore important to keep the sextupole strengths low to minimize any residual aberrations.

Analysis of the various sextupole schemes using MAD showed that the optimum sextupole locations are at the horizontally focusing quadrupoles in the first two and last two cells in the arc. Sextupole strengths are at minimum at these locations and are listed in Table 3. Phase advance between sextupoles in each pair is equal to the cell phase advance: $\mu_x = 108°, \mu_y = 72°$.

Chromatic W-functions and second order dispersion after correction are shown in Fig. 24 and 25, respectively. Compared to Fig. 21, the sextupoles did not have significant impact on W-functions, and therefore should not have increased contribution to emittance growth from betatron chromaticity.

As shown in Fig. 25, the corrected second order dispersion is perfectly periodic in the compressor arc, and the second order chicane bumps are naturally closed. Tracking with the sextupoles has been performed and the resultant chromatic bandwidth is shown in Fig. 26 and 27 for the nominal and

Table 3: Sextupole parameters at 8 GeV for the modified pre-linac bunch compressor section.

Magnet	Number	Length (m)	Pole-tip field (kG)	Aperture (cm)
Sextupole				
SDX1	2	0.21	0.2567	1.0
SDX2	2	0.21	0.2412	1.0

10 times larger emittance, respectively. The horizontal emittance growth is significantly reduced compared to Fig. 23 which confirms that the residual second order dispersion was the cause of emittance growth. Fig. 27 also shows that sextupole geometric aberrations are minimal as a result of low sextupole strengths.

We conclude that it is desirable to provide a sextupole correction of the second order dispersion for the bunch compressor section to attain a better chromatic bandwidth. Presently, the arc cells do not have enough space for the sextupoles. In the study, we artificially split the sextupoles in two halves and placed them at either side of the corresponding quadrupoles. For a realistic design, the arc cells may need to be modified to provide space for the sextupoles. For a compact design, short sextupoles may be used since their strengths are low as listed in Table 3.

References

[1] The NLC Design Group, "*Zeroth-Order Design Report for the Next Linear Collider*," LBNL-PUB-5424, SLAC Report 474, UCRL-ID-124161, UC-414 (1996).

[2] NLC optics decks on the web, http://www-project.slac.stanford.edu/lc/local/AccelPhysics/Accel_Physics_index.htm.

[3] P. Tenenbaum, *et al.*, "*Use of Simulation Programs for the Modeling of the Next Linear Collider*," SLAC–PUB–8136 (1999).

[4] The MAD Home Page, http://wwwslap.cern.ch/mad/.

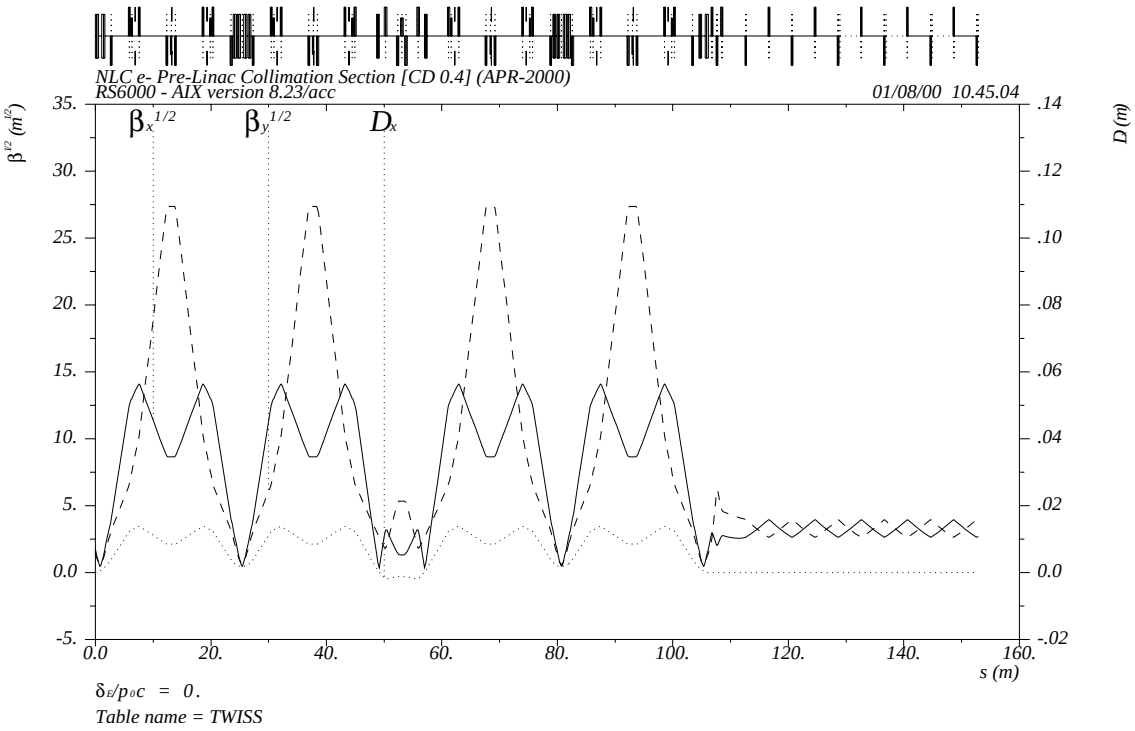

Figure 1: Lattice functions in the ZDR type pre-linac collimation section.

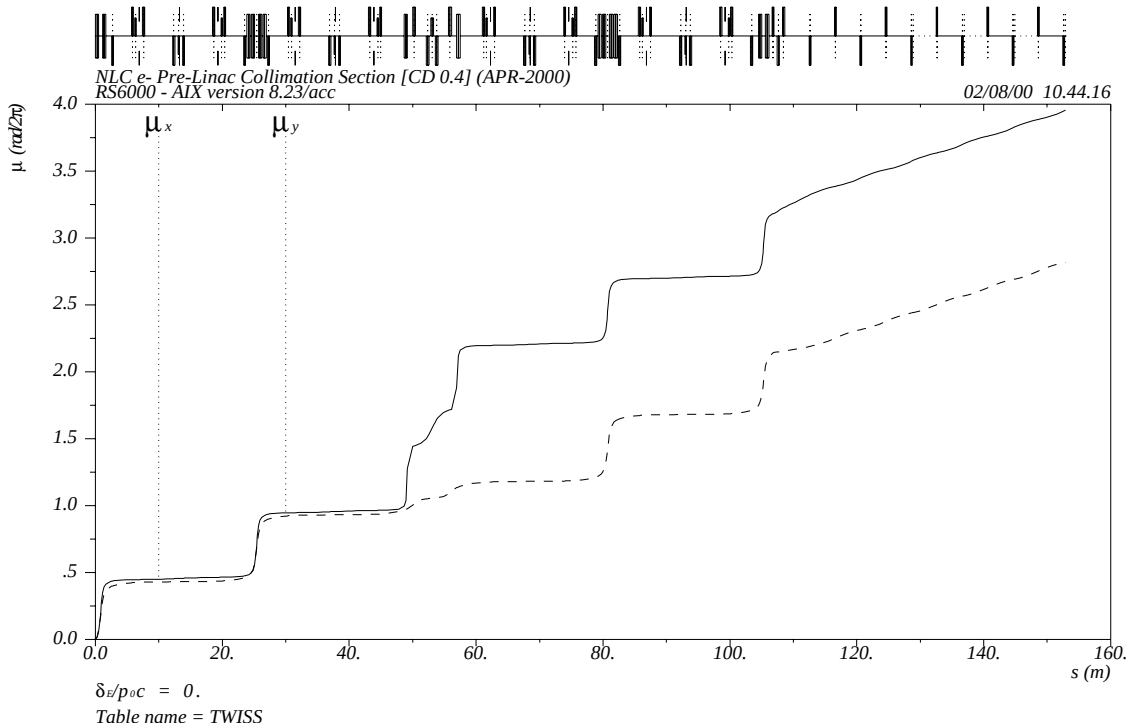

Figure 2: Phase advance $\mu/2\pi$ in the ZDR type pre-linac collimation section.

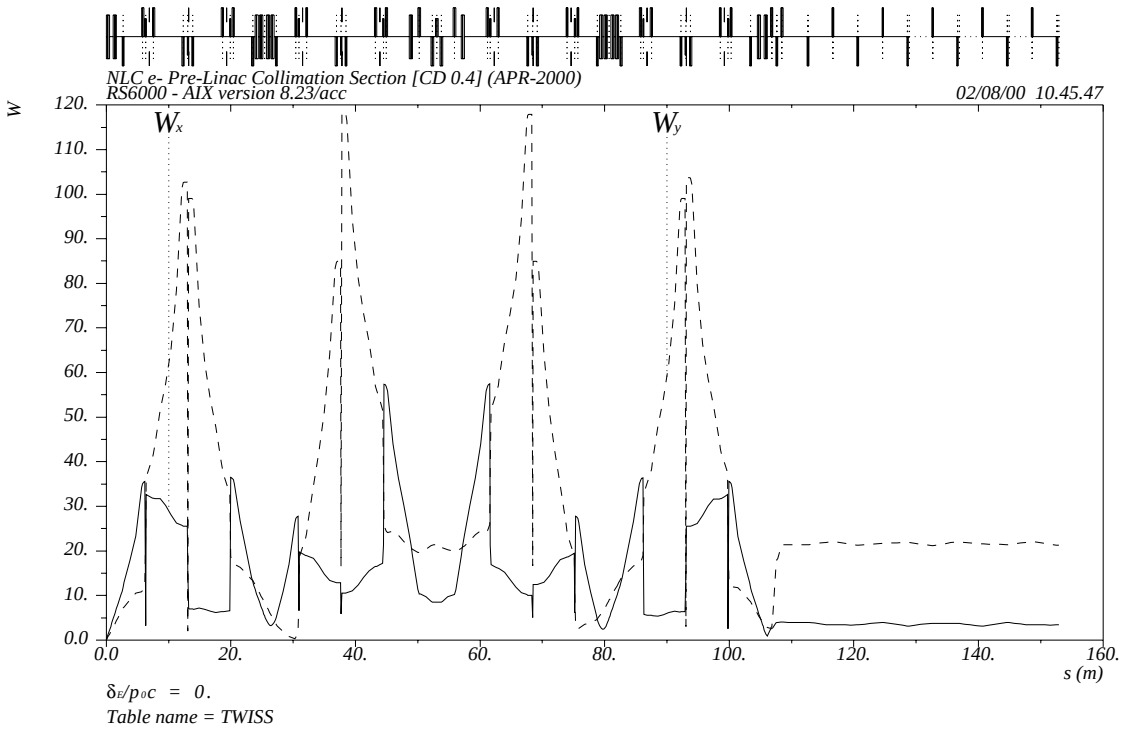

Figure 3: W-functions in the ZDR type pre-linac collimation section.

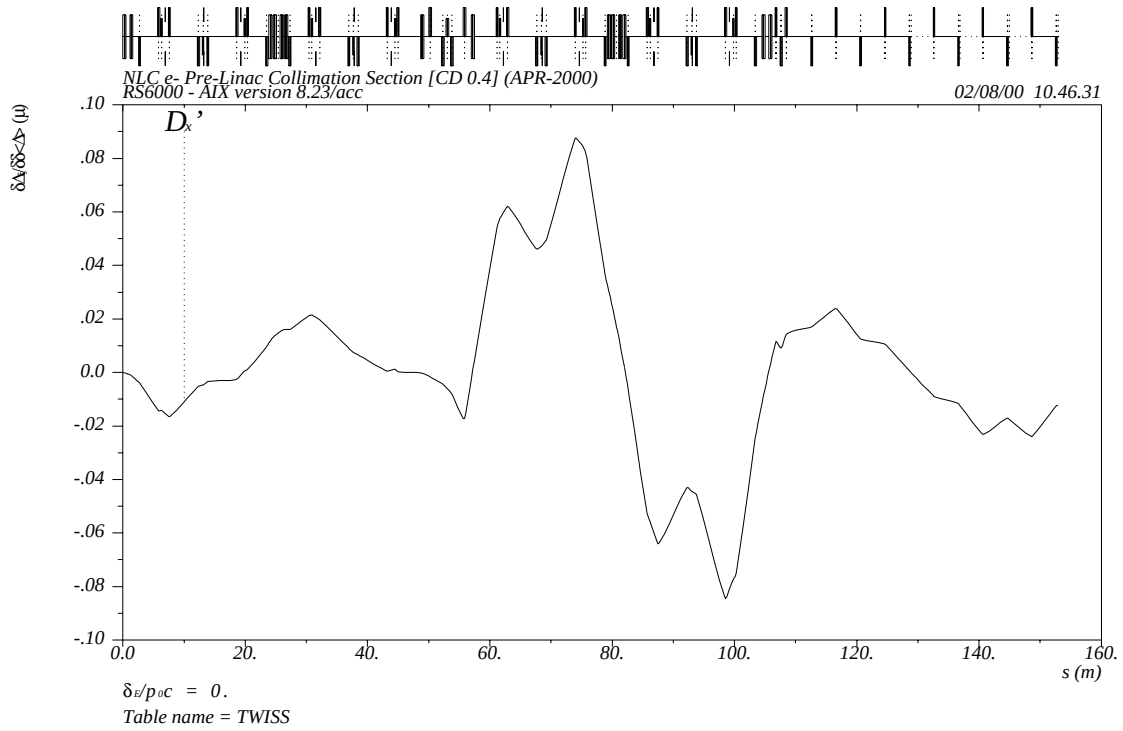

Figure 4: Second order dispersion in the ZDR type pre-linac collimation section.

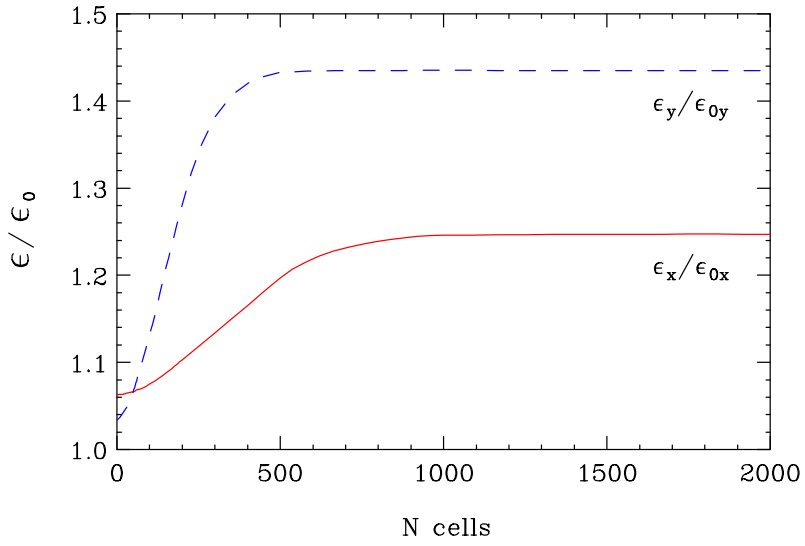

Figure 5: Example of emittance filamentation in the ZDR type pre-linac collimation section with N diagnostic cells. $E=8$ GeV, $\gamma\epsilon_{0x}=3\cdot10^{-6}m$, $\gamma\epsilon_{0y}=3\cdot10^{-8}m$, $\sigma_\delta=0.26\%$, $\delta=-4\%$.

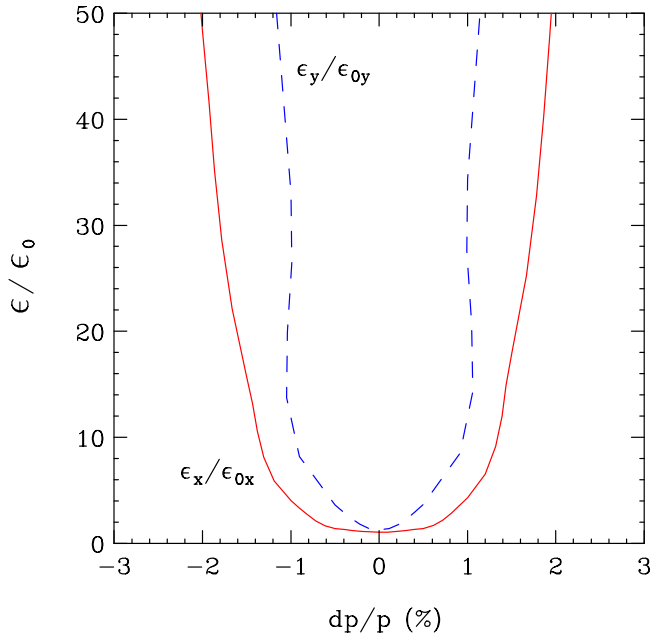

Figure 6: Effective emittance growth in the ZDR type pre-linac collimation section with bends and sextupoles turned off. $E=8$ GeV, $\gamma\epsilon_{0x}=3\cdot10^{-6}m$, $\gamma\epsilon_{0y}=3\cdot10^{-8}m$, $\sigma_\delta=0.26\%$.

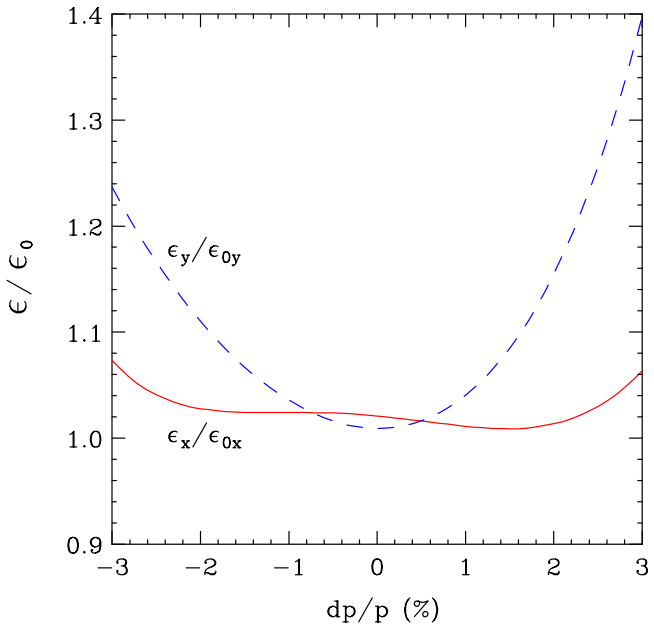

Figure 7: Effective emittance growth in the ZDR type pre-linac collimation section. $E = 8$ GeV, $\gamma\epsilon_{0x} = 3 \cdot 10^{-6} m$, $\gamma\epsilon_{0y} = 3 \cdot 10^{-8} m$, $\sigma_\delta = 0.26\%$.

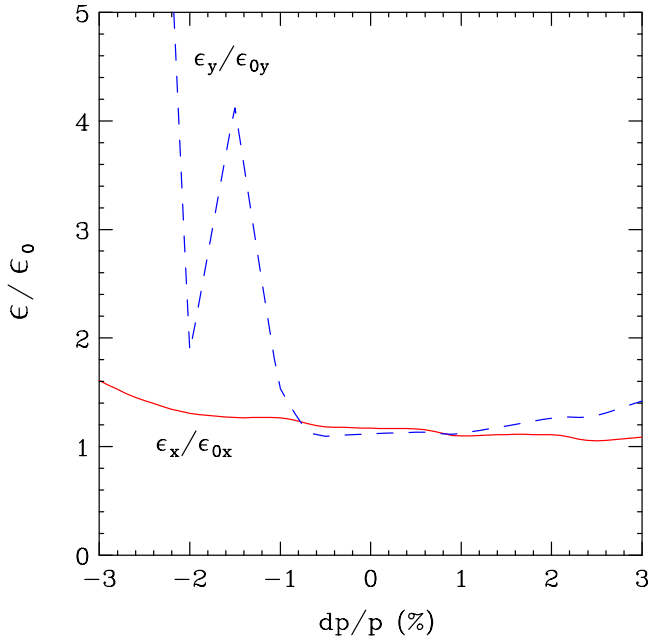

Figure 8: Effective emittance growth in the ZDR type pre-linac collimation section for 10 times larger initial emittance. $E = 8$ GeV, $\gamma\epsilon_{0x} = 3 \cdot 10^{-5} m$, $\gamma\epsilon_{0y} = 3 \cdot 10^{-7} m$, $\sigma_\delta = 0.26\%$.

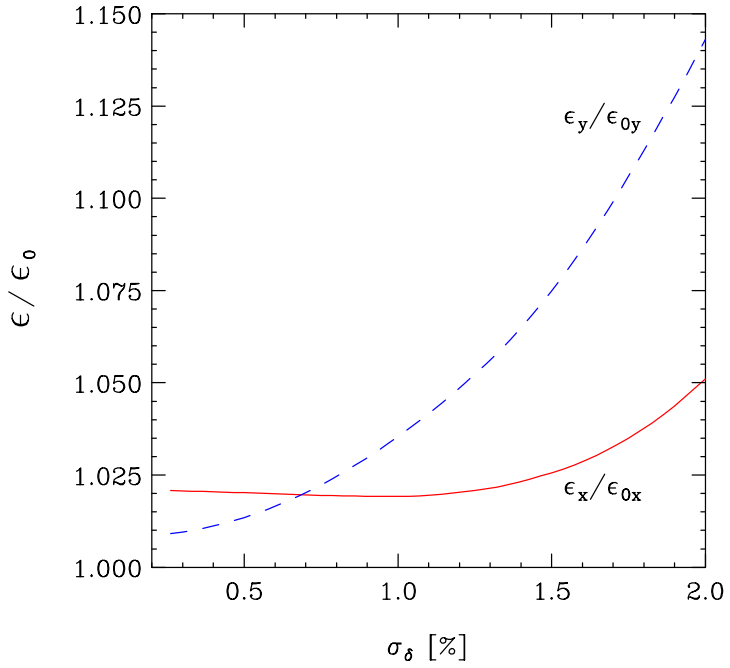

Figure 9: Effective emittance growth in the ZDR type pre-linac collimation section vs. *rms* energy spread. $E = 8$ GeV, $\gamma\epsilon_{0x} = 3 \cdot 10^{-6} m$, $\gamma\epsilon_{0y} = 3 \cdot 10^{-8} m$.

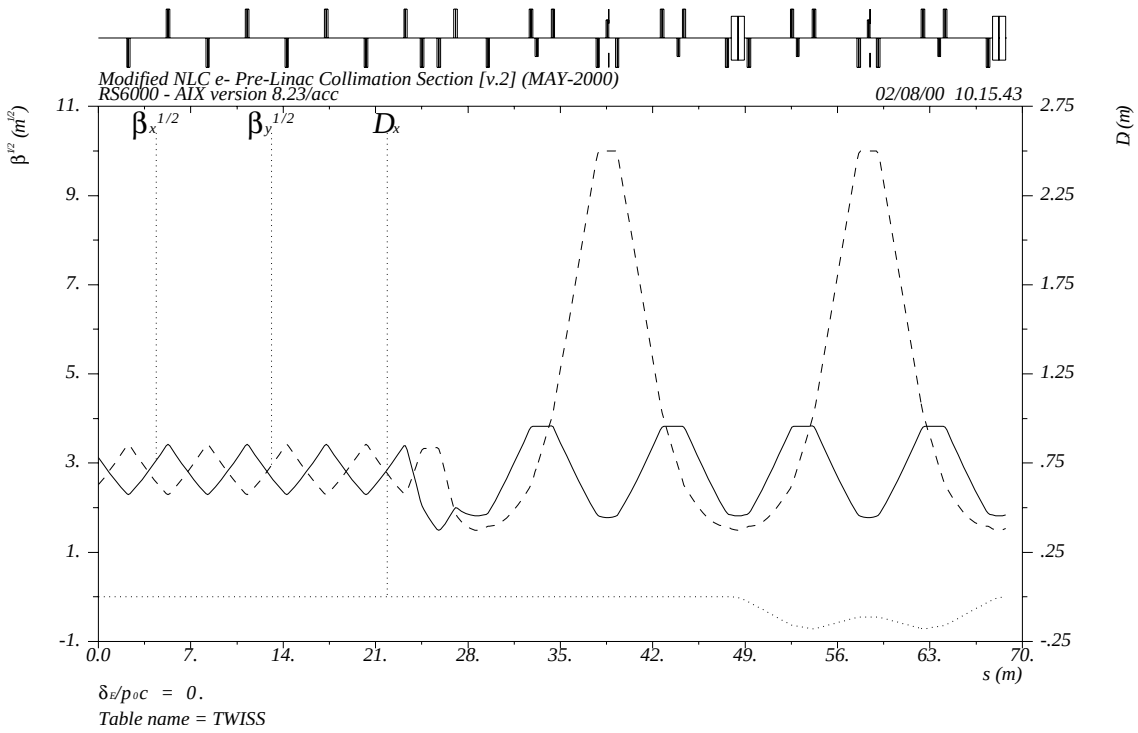

Figure 10: Lattice functions in the modified NLC pre-linac collimation section.

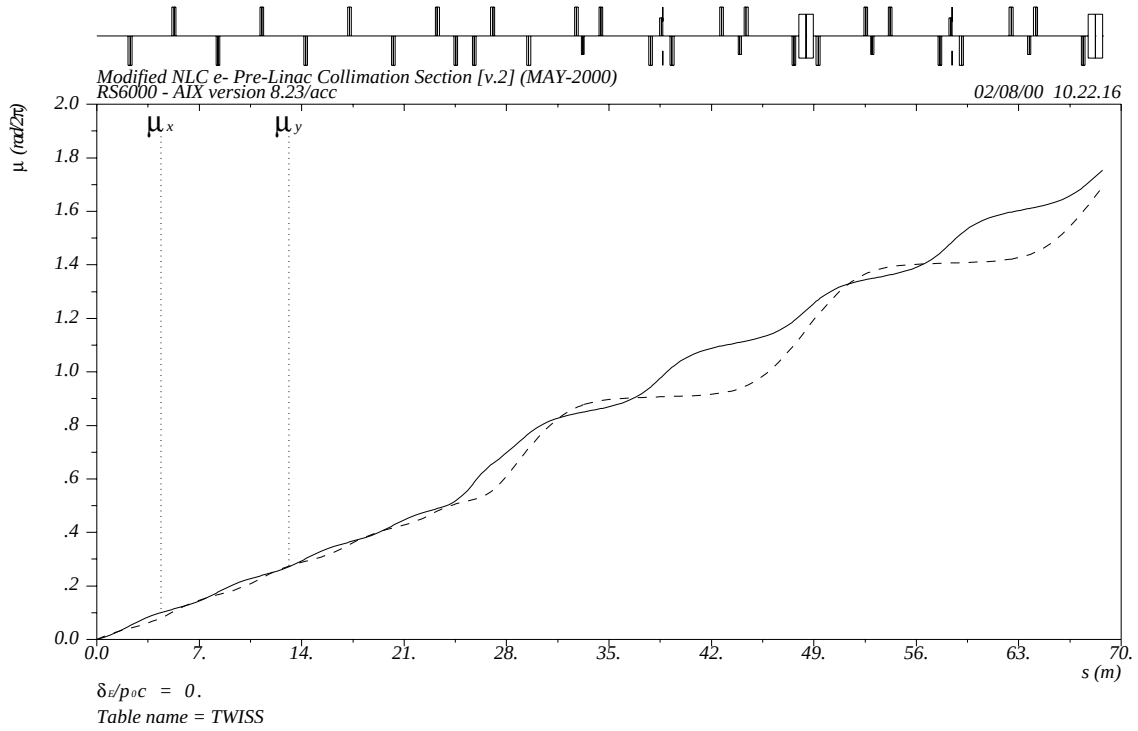

Figure 11: Phase advance $\mu/2\pi$ in the modified NLC pre-linac collimation section.

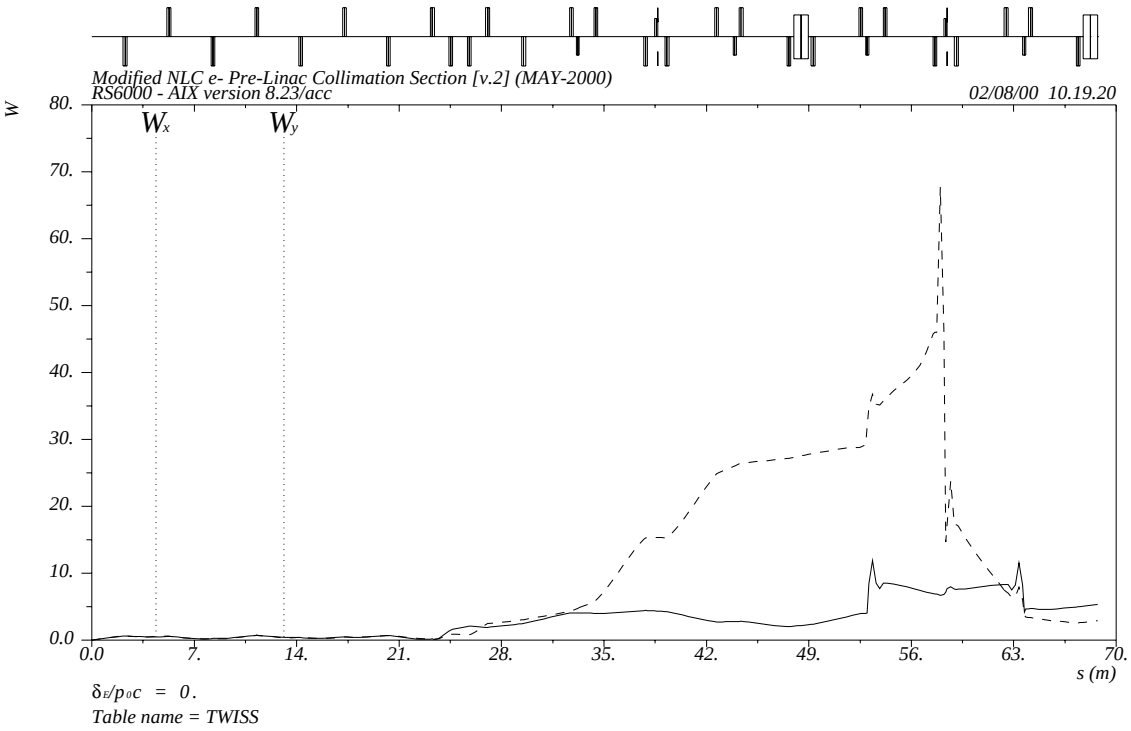

Figure 12: W-functions in the modified NLC pre-linac collimation section.

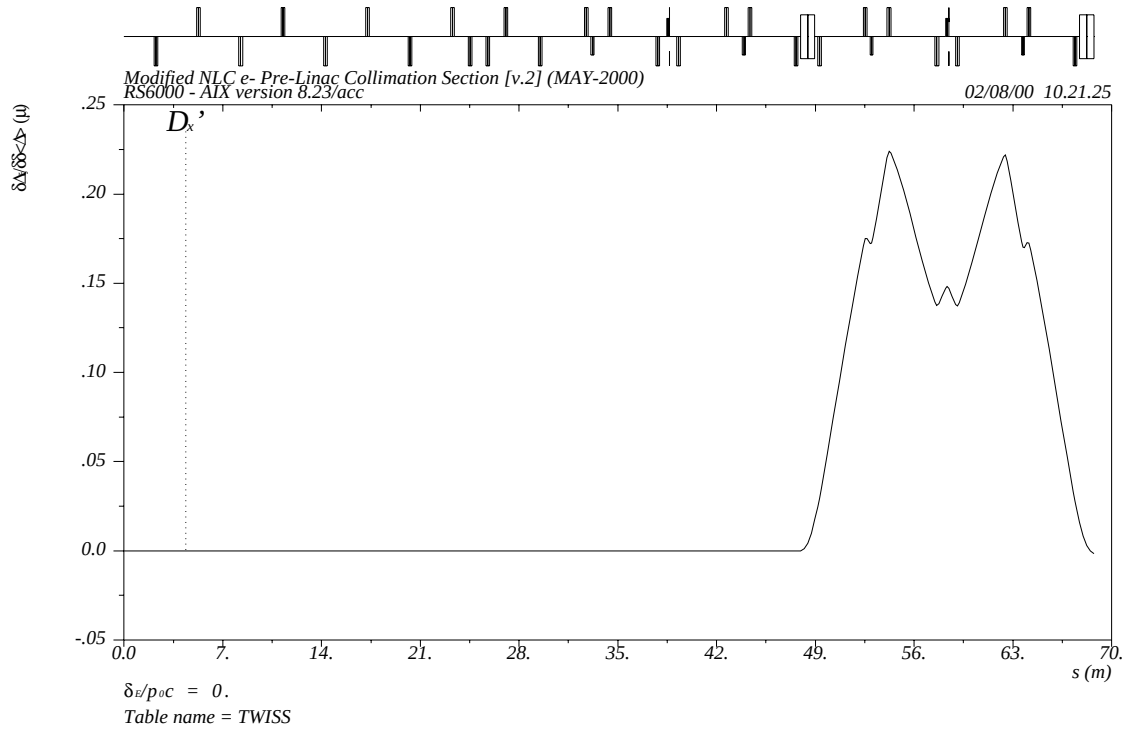

Figure 13: Second order dispersion in the modified NLC pre-linac collimation section.

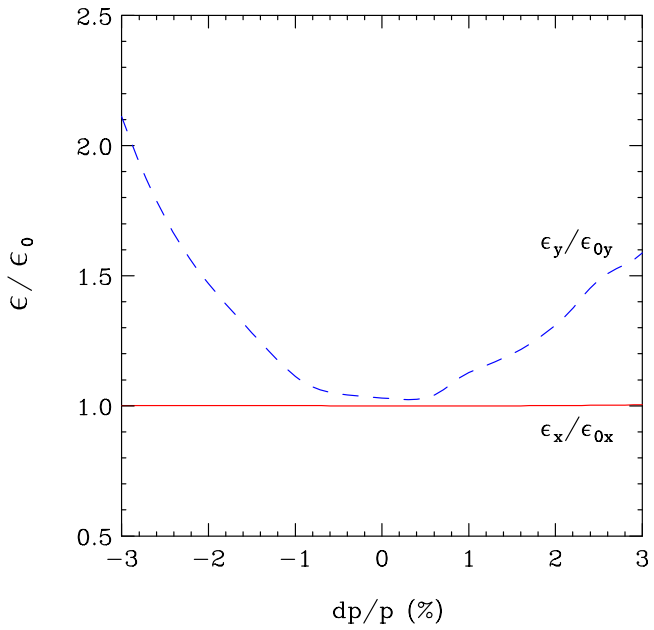

Figure 14: Effective emittance growth in the modified NLC pre-linac collimation section with bends and sextupoles turned off. $E=8$ GeV, $\gamma\epsilon_{0x}=3\cdot10^{-6}m$, $\gamma\epsilon_{0y}=3\cdot10^{-8}m$, $\sigma_\delta=0.26\%$.

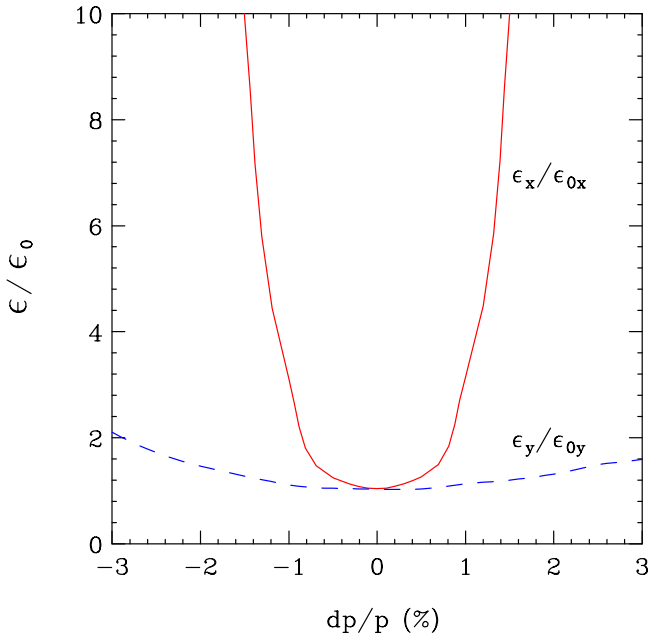

Figure 15: Effective emittance growth in the modified NLC pre-linac collimation section with sextupoles turned off. $E=8$ GeV, $\gamma\epsilon_{0x}=3\cdot10^{-6}m$, $\gamma\epsilon_{0y}=3\cdot10^{-8}m$, $\sigma_\delta=0.26\%$.

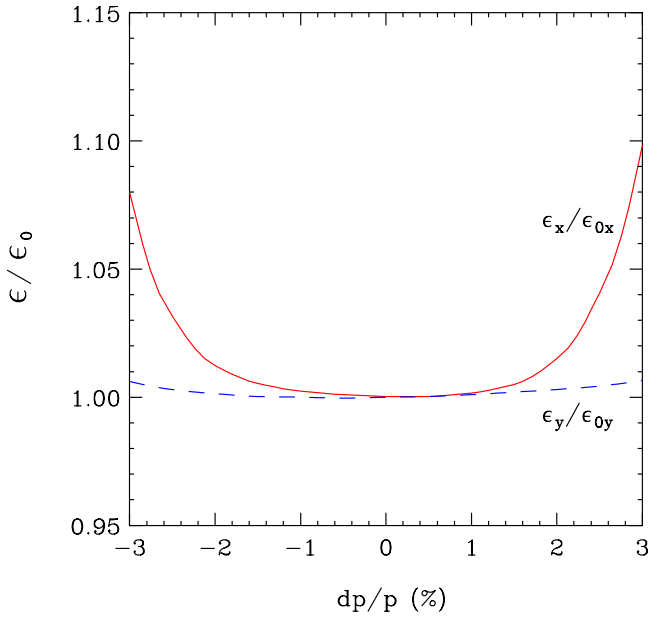

Figure 16: Effective emittance growth in the modified NLC pre-linac collimation section. $E = 8$ GeV, $\gamma\epsilon_{0x} = 3 \cdot 10^{-6} m$, $\gamma\epsilon_{0y} = 3 \cdot 10^{-8} m$, $\sigma_\delta = 0.26\%$.

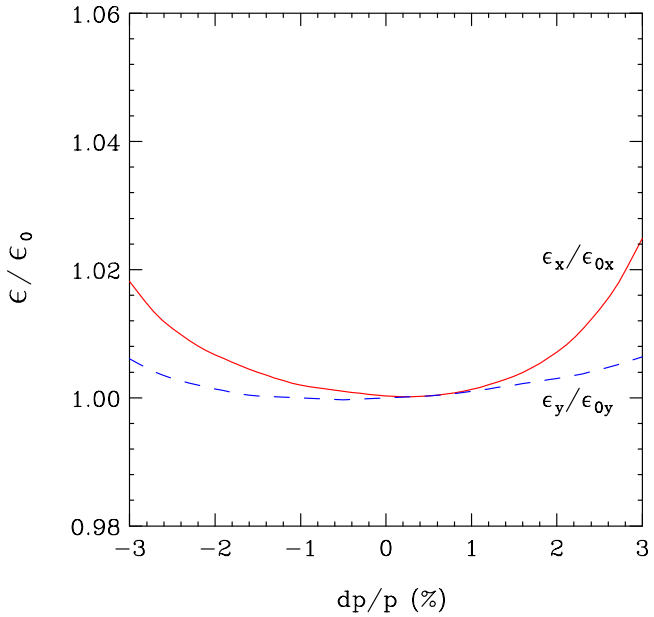

Figure 17: Effective emittance growth in the modified NLC pre-linac collimation section for 10 times larger initial emittance. $E = 8$ GeV, $\gamma\epsilon_{0x} = 3 \cdot 10^{-5} m$, $\gamma\epsilon_{0y} = 3 \cdot 10^{-7} m$, $\sigma_\delta = 0.26\%$.

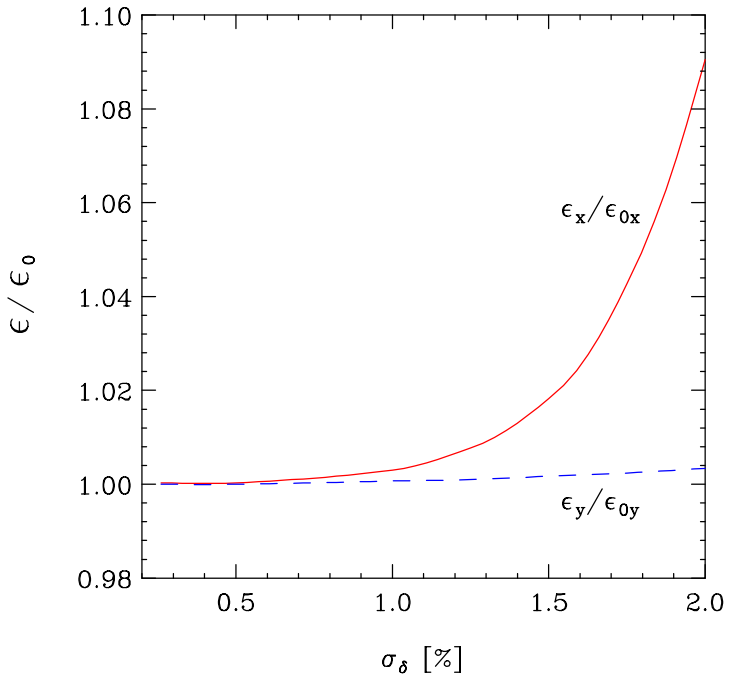

Figure 18: Effective emittance growth in the modified NLC pre-linac collimation section vs. *rms* energy spread. $E=8$ GeV, $\gamma\epsilon_{0x}=3\cdot10^{-6}m$, $\gamma\epsilon_{0y}=3\cdot10^{-8}m$.

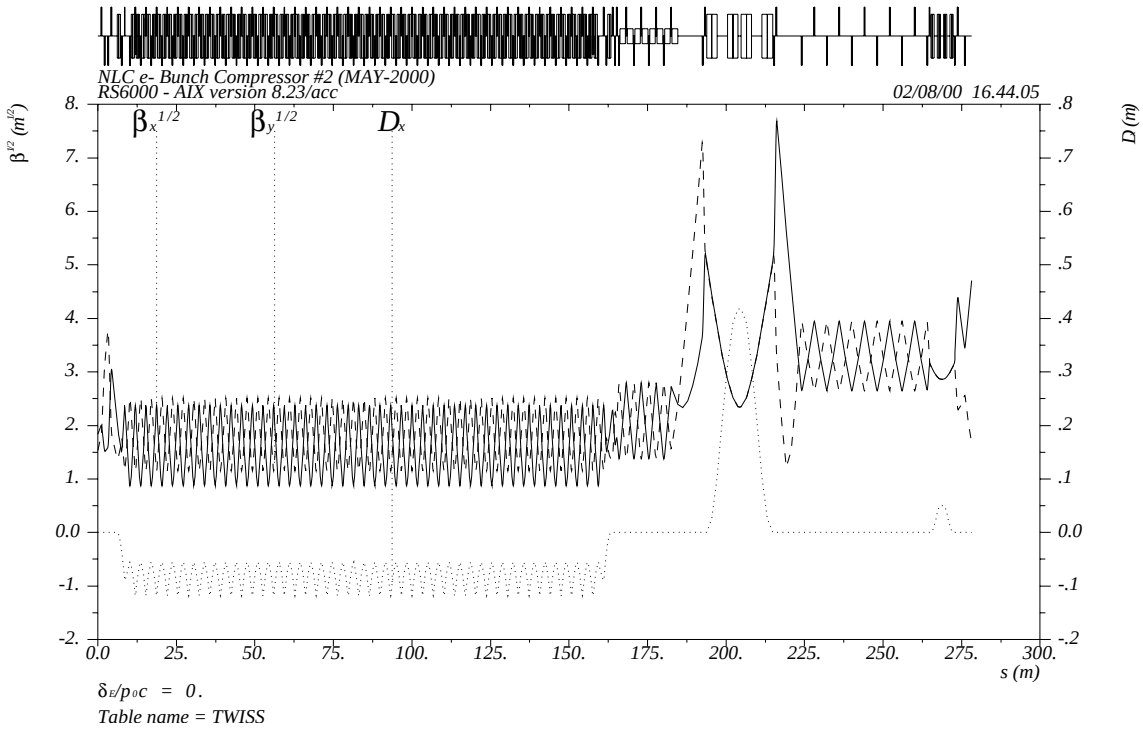

Figure 19: Lattice functions in the NLC pre-linac bunch compressor.

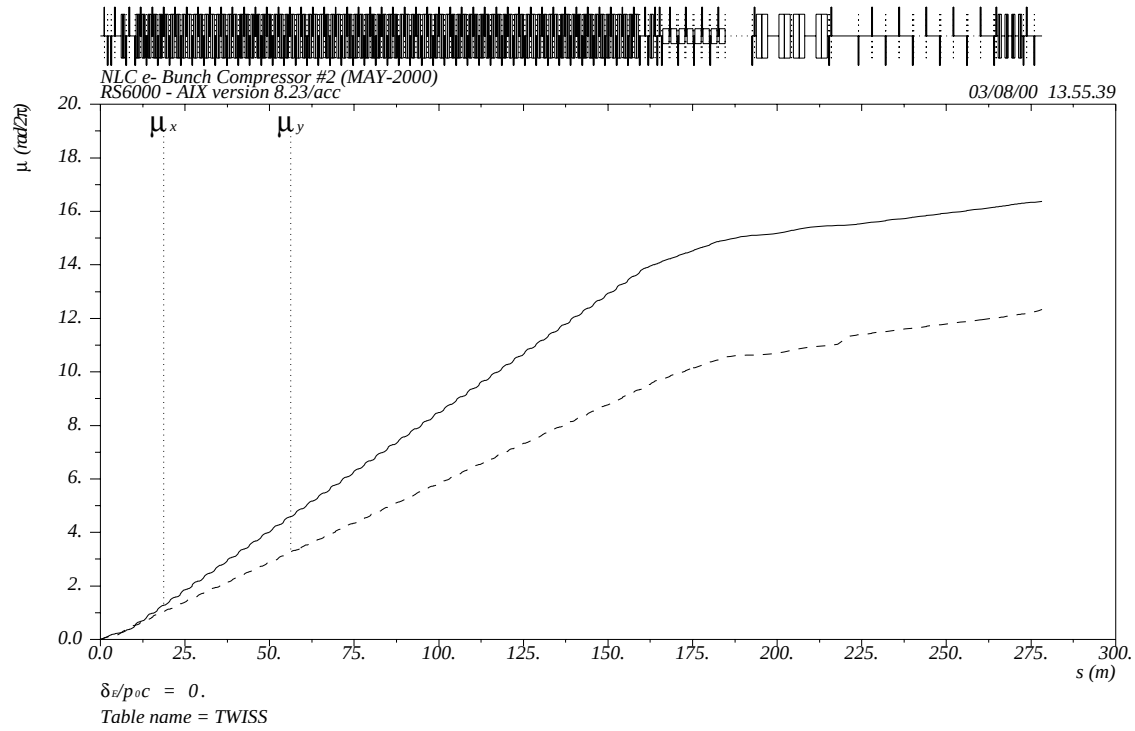

Figure 20: Phase advance $\mu/2\pi$ in the NLC pre-linac bunch compressor.

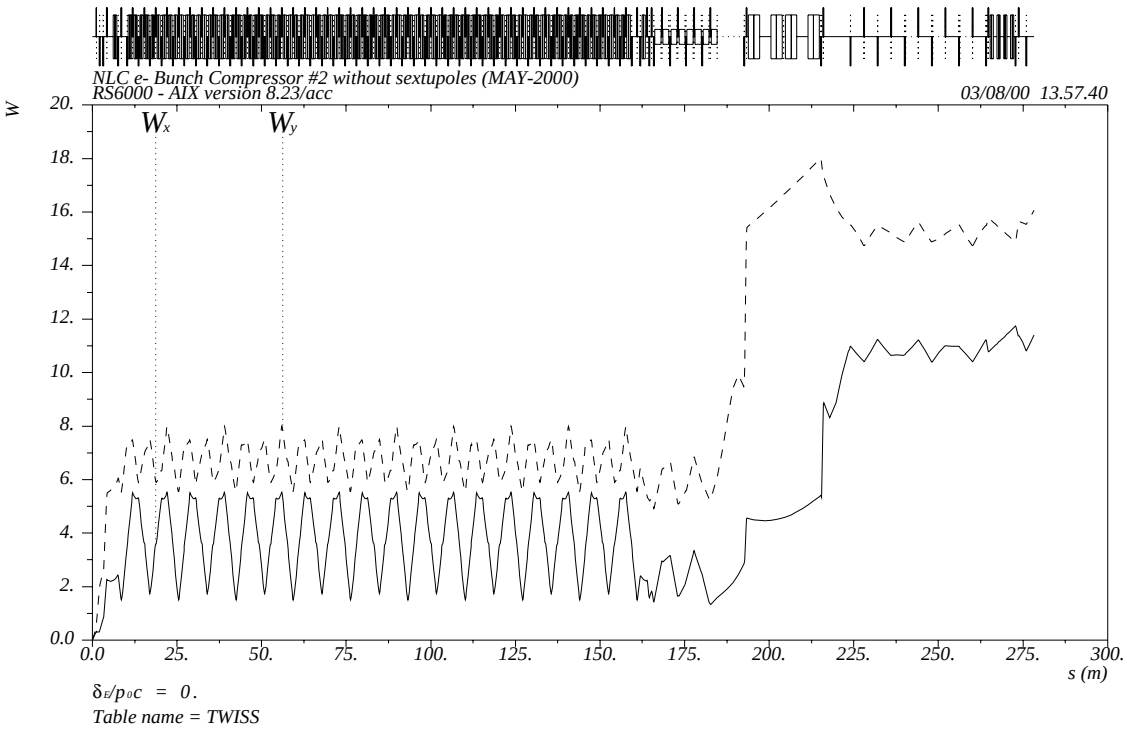

Figure 21: W-functions in the NLC pre-linac bunch compressor without sextupoles.

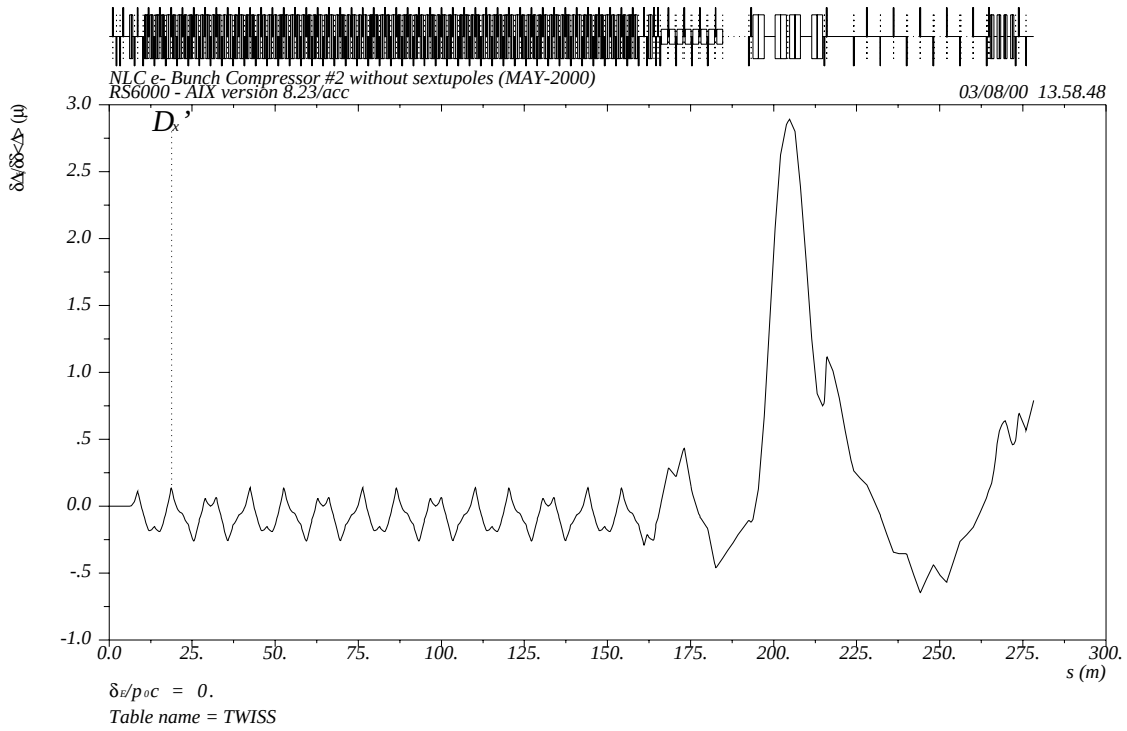

Figure 22: Second order dispersion in the NLC pre-linac bunch compressor without sextupoles.

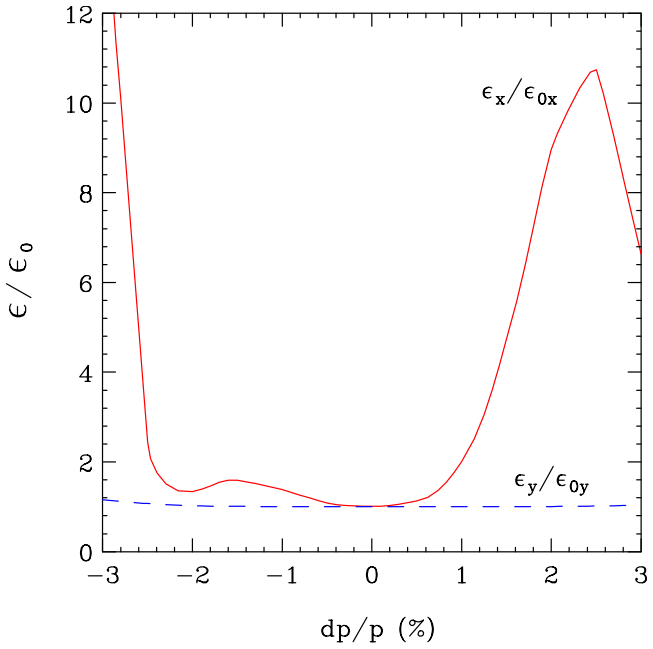

Figure 23: Effective emittance growth in the NLC pre-linac bunch compressor without sextupoles. $E = 8$ GeV, $\gamma\epsilon_{0x} = 3 \cdot 10^{-6} m$, $\gamma\epsilon_{0y} = 3 \cdot 10^{-8} m$, $\sigma_\delta = 0.26\%$.

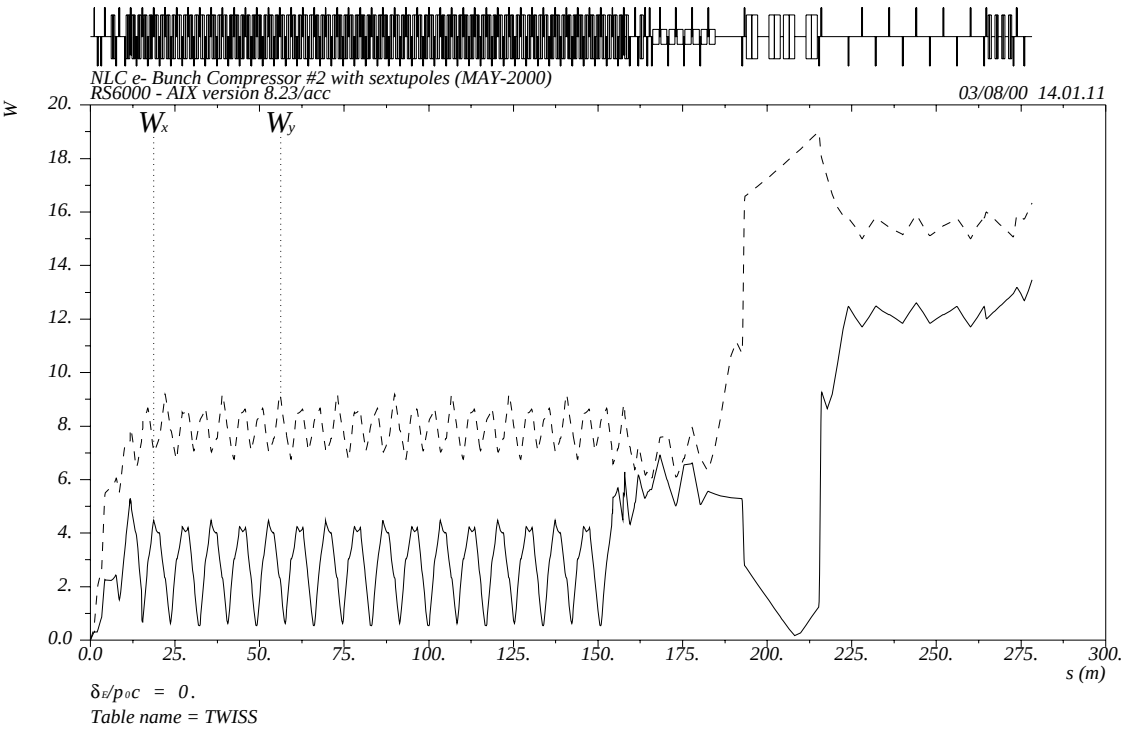

Figure 24: W-functions in the NLC pre-linac bunch compressor with sextupoles.

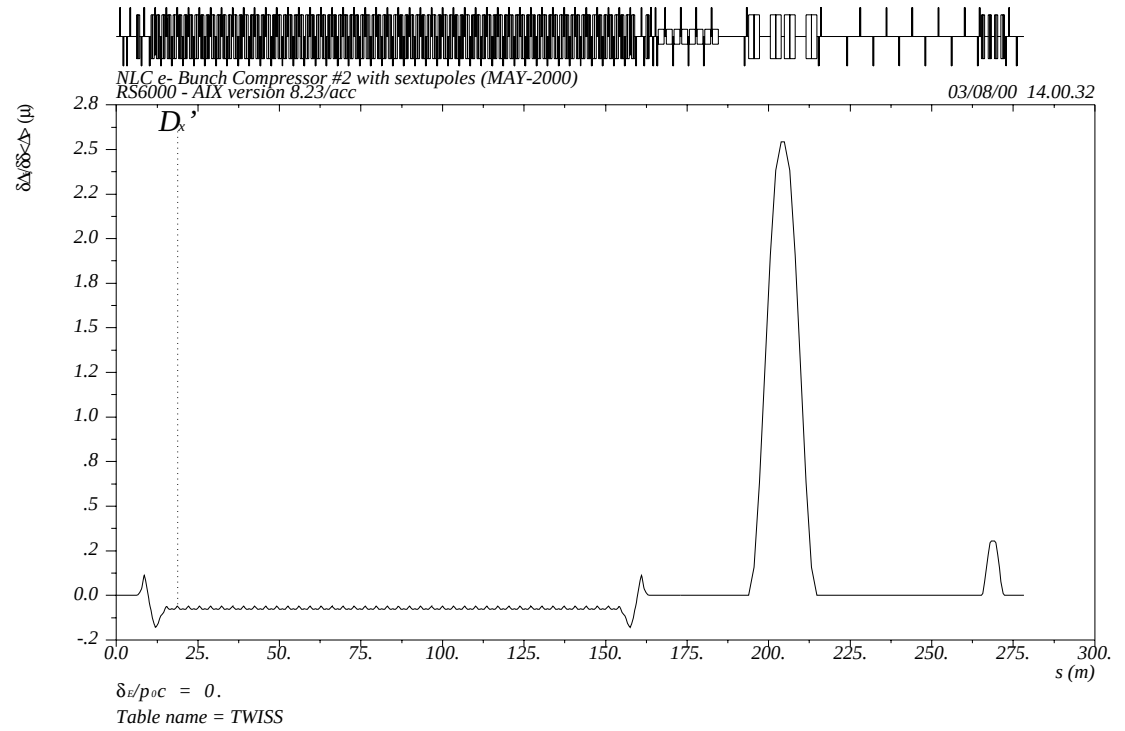

Figure 25: Second order dispersion in the NLC pre-linac bunch compressor with sextupoles.

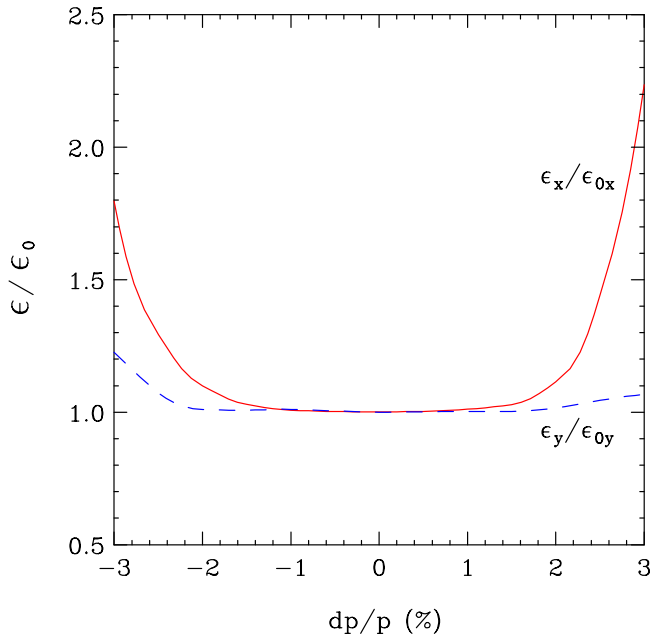

Figure 26: Effective emittance growth in the NLC pre-linac bunch compressor with sextupoles. $E=8$ GeV, $\gamma\epsilon_{0x}=3\cdot10^{-6}m$, $\gamma\epsilon_{0y}=3\cdot10^{-8}m$, $\sigma_\delta=0.26\%$.

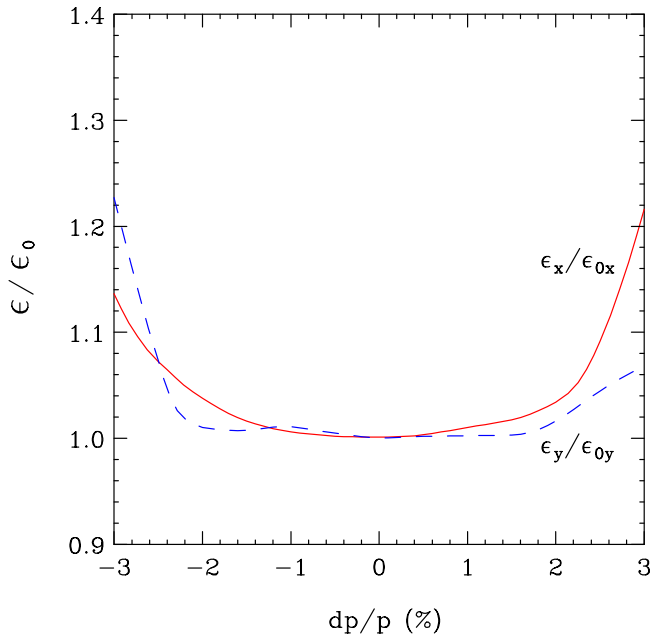

Figure 27: Effective emittance growth in the NLC pre-linac bunch compressor with sextupoles for 10 times larger initial emittance. $E=8$ GeV, $\gamma\epsilon_{0x}=3\cdot10^{-5}m$, $\gamma\epsilon_{0y}=3\cdot10^{-7}m$, $\sigma_\delta=0.26\%$.